


 Cite this: *RSC Adv.*, 2025, 15, 26353

Substrate temperature modulated optical characterizations of α - CdIn_2Se_4 thin films grown by pulsed laser deposition technique

 S. D. Dhruv,^a Tanvi Dudharejija,^b Sergei A. Sharko,^c Aleksandra I. Serokurova,^c Nikolai N. Novitskii,^c D. L. Goroshko,^d Parth Rayani,^{ae} Jagruti Jangale,^a Vanaraj Solanki,^f P. B. Patel,^g U. B. Trivedi,^g J. H. Markna,^b Bharat Kataria^b and D. K. Dhruv^{*a}

The current study examines the effect of substrate temperature (T_s) on the optical characteristics of CdIn_2Se_4 thin films grown by the pulsed laser deposition technique using a UV-Vis-NIR spectrophotometer. Transmittance maxima of CdIn_2Se_4 thin films shift with a change in T_s , exhibit high absorption in the visible region, and depict an absorption coefficient (α) of $\approx 10^7 \text{ m}^{-1}$. Refractive index spectra of CdIn_2Se_4 thin films controlled by T_s reflect crests at characteristic wavelengths (λ_c) and a wavelength (λ) higher than λ_c ; spectra display normal dispersion. The extinction coefficient (k) of T_s tempered CdIn_2Se_4 thin films decreases as λ increases and reaches a minimum at λ_c ; the contribution of free carrier absorption can explain the increase in k values after λ_c . The effect of T_s on the optical band gap energy (E_g) of the CdIn_2Se_4 thin films is discussed. For T_s -modulated CdIn_2Se_4 thin films, dielectric constants, loss tangent, Urbach energy, Urbach absorption coefficient, and optical and electrical conductivities have been inferred. Peak values of the volume and surface energy loss functions of CdIn_2Se_4 thin films were retrieved. A Fourier transform infrared spectrophotometer verified the purity of CdIn_2Se_4 thin films formed at different T_s . The current study indicates that CdIn_2Se_4 thin films are promising options for designing and developing upcoming high-efficiency opto-electronic devices. Implications are discussed.

 Received 1st June 2025
 Accepted 17th July 2025

DOI: 10.1039/d5ra03888j

rsc.li/rsc-advances

1 Introduction

Due to their potential uses in thermo-electric materials,¹ semiconductor instrumentation,² switching devices,^{3,4} photocatalysts,^{5–7} photoconductors,^{8,9} non-linear optical devices,^{10,11} optical filters,¹² optoelectronics,¹³ solar cells,^{14–17} and more, ternary semiconducting compounds with the composition $\text{II-III}_2\text{-VI}_4$ (where $\text{II} = \text{Zn, Cd, or Hg}$; $\text{III} = \text{Al, Ga, or}$

In ; $\text{VI} = \text{S, Se, or Te}$) have been studied extensively over the globe since 1955.¹⁸ $\text{II-III}_2\text{-VI}_4$ group compounds are earth-abundant, less expensive, and less toxic; they are largely derived from the zinc blende structure using the Grimm–Sommerfel rule. According to Hahn *et al.*,¹⁸ ternary semiconducting compounds of composition $\text{II-III}_2\text{-VI}_4$ have a space group $S_4^2(I\bar{4})$. They are thiogallates that crystallize into a tetragonal structure¹⁹ and are distinguished from chemical and iso-electronic analogs with the structure of chalcopyrite and sphalerite by the presence of an ordered cation vacancy. As a result, compounds of composition $\text{II-III}_2\text{-VI}_4$ are known as defective chalcopyrite (DC).

The $\text{II-III}_2\text{-VI}_4$ family's CdIn_2Se_4 has enthralled substantial contemplation from scientists over the orb due to its prerogatives in thermoelectric materials,^{20,21} photoanodes,²² hetero-junction solar cells,²³ PEC solar cells,^{24–28} photovoltaics,²⁹ *etc.* The structural, morphological, electrical, optical, mechanical, vibrational, and thermoelectric properties of CdIn_2Se_4 in bulk and/or thin film form have been explored by various authors.^{30–34} Experimental studies of the ordered-vacancy compound CdIn_2Se_4 have revealed that its tetragonal structure can be deformed with a lattice constant ratio c/a of 1, 2, and 3, which are referred to as the α (pseudo-cubic), β , and γ phases, respectively, depending on the synthesis conditions.³¹ Because

^aNatubhai V. Patel College of Pure and Applied Sciences, The Charutar Vidya Mandal (CVM) University, Vallabh Vidyanagar-388120, Anand, Gujarat, India. E-mail: dhananjaydhruv@rediffmail.com

^bDepartment of Nanoscience and Advanced Materials, Saurashtra University, Rajkot-360005, Gujarat, India

^cLaboratory of Magnetic Films Physics, Scientific-Practical Materials Research Centre of National Academy of Sciences of Belarus, 220072 Minsk, Belarus

^dInstitute of Automation and Control Processes Far Eastern Branch of the Russian Academy of Sciences, 5 Radio St., Vladivostok 690041, Russia

^eGovernment Science College, Maharaja Krishnakumarsinhji Bhavnagar University, Gariyadhar-364505, Bhavnagar, Gujarat, India

^fDr K. C. Patel R & D Centre, Charotar University of Science and Technology, Changa-388421, Gujarat, India

^gDepartment of Electronics, Sardar Patel University, Vallabh Vidyanagar-388120, Anand, Gujarat, India



of their high absorption coefficient, optical band gap energy (E_g) in the visible spectra, and relatively high photo-electronic sensitivity from the visible to the near-infrared spectrum range, CdIn₂Se₄ thin films are a propitious entrant for photonic devices. As an upshot, research on their optical characteristics is of prodigious concern.

When depositing ternary semiconducting compounds with constituents that have varying vapor pressures, pulsed laser deposition (PLD) is an excellent choice. Comparing PLD technology to traditional vacuum-based thin film deposition methods, the former reduces processing times by enabling the growth of uniform and fast thin films. Of particular relevance is the ease with which heterojunctions and multilayer structures requiring precise control over film thickness can be produced using PLD technology. In the current study, the authors employed PLD to deposit CdIn₂Se₄ thin films because it offers several benefits over other thin film deposition methods, such as outstanding thickness controllability, broad universality, high-level cleanliness in the deposited film, and reproducible maintenance of the target material's precise composition.^{35,36}

In the current study, amorphous quartz glass (fused silica) was employed to deposit CdIn₂Se₄ thin films for their optical characterization. Due to its excellent transparency in the UV-Visible-NIR spectra, quartz glass is perfect for examining the optical characteristics of thin films without the substrate affecting the results. Characterizing the thin film's intrinsic optical behavior is easier because quartz glass is non-crystalline and does not introduce diffraction patterns or crystallographic effects. Because it does not react with many solvents and can tolerate high processing temperatures, quartz is useful for post-treatment and film deposition procedures. The smooth surface of high-quality quartz glass usually aids in producing homogeneous films and reliable optical data.

In the extant investigation, an attempt has been made to acquire exhaustive information on the effect of substrate temperature (T_s) on the optical properties of pulsed laser deposited α -phase CdIn₂Se₄ thin films by engaging sophisticated techniques such as ultraviolet-visible-near infrared (UV-VIS-NIR) and Fourier transform infrared (FTIR) spectrophotometers by keeping CdIn₂Se₄ thin film's thickness (d) identical throughout the investigation. The authors believe that the contemporary enquiry on the hitherto unfabricated-unpublished-unreported, T_s -controlled optical characterizations of pulsed laser deposited α -phase CdIn₂Se₄ thin films should not only be an accumulation to the prevailing list but also lead to the further understanding of the optical properties of thin films and the research will afford optimized optical parameters for designing and developing of future novel semiconducting compound thin film opto-electronic device applications.

2 Experimental

For their optical characterizations, CdIn₂Se₄ ternary semiconducting compound thin films were deposited using the PLD technique (model: Compex-Pro Excimer Laser 102F; make: Coherent, Germany). The source (target) material was a single-

phase CdIn₂Se₄ (ref. 37) in a pellet form with 10 mm (diameter) \times 3 mm (thickness) dimensions. The substrates were ultrasonically cleaned amorphous quartz glass (make: Blue Star, made: Polar Industries Corporation, India) with dimensions 10 ± 0.1 mm (length) \times 3 ± 0.1 mm (breadth) \times 1.45 ± 0.1 mm (thickness). A CdIn₂Se₄ pellet and amorphous quartz glass were mounted in a stainless-steel PLD chamber (make: Excel Instruments, India). Silver conductive adhesive paste (model: RS pro-RS186-3600, made: RS Components & Controls Limited, India) adheres the CdIn₂Se₄ pellet to the target holder and amorphous quartz glass substrates to the substrate holder. The CdIn₂Se₄ pellet was irradiated by a krypton fluoride (KrF) pulsed laser through a quartz lens. The plasma plume dimension at the CdIn₂Se₄ pellet was optimized and confined using a quartz lens. 45° separates the substrate holder from the incident laser that catarracts on the target. The target was spun at six revolutions per minute (rpm) during laser ablation to avert mutilation from dropping laser stuck at a single spot incessantly on the CdIn₂Se₄ target.

The thin films of CdIn₂Se₄ were deposited on the amorphous quartz glass substrate at diverse T_s , vacillating from room temperature (RT) (≈ 300 K) to 675 K ($300 \text{ K} \leq T_s \leq 675 \text{ K}$) using a calibrated chromel–alumel (Cr–Al) thermocouple abetted microcontroller-based temperature controller (make: Coherent, India). The T_s were sensed and controlled during the thin film deposition by mounting the chromel–alumel (Cr–Al) thermocouple on the quartz glass substrate surface. The thin film d and deposition rate was monitored and/or controlled by the *in situ* digital quartz crystal thickness monitor (model: DTM-101, make: Hind High Vacuum Co. Pvt. Ltd, India). During CdIn₂Se₄ thin films' deposition, the evaporation rate ($\approx 10 \text{ nm s}^{-1}$) and the d of the deposits ($\approx 100 \text{ nm}$) were kept constant. Table 1 displays the PLD parameters optimized for synthesizing CdIn₂Se₄ thin films.

The variable laser ablation duration was used to achieve consistent d at all T_s . It was observed that the thin films deposited at lower T_s require less laser ablation time during the synthesis of thin films, whereas thin films synthesized at higher T_s require more laser ablation time to achieve the same d as those deposited at lower T_s because of re-evaporation at high T_s .

The effect of the T_s ($300 \text{ K} \leq T_s \leq 675 \text{ K}$) on the optical properties of pulsed laser deposited CdIn₂Se₄ thin films was scrutinized by recording room temperature (RT) ($\approx 300 \text{ K}$) transmittance ($T(\lambda)$) spectra employing UV-Vis-NIR

Table 1 PLD parameters optimized for the synthesis of CdIn₂Se₄ thin films

| S. no. | Parameter | Value |
|--------|---------------------------------------|---|
| 1 | KrF laser wavelength (λ) | $\approx 248 \text{ nm}$ |
| 2 | KrF laser energy | $\approx 255 \text{ mJ}$ |
| 3 | Repetition rate (frequency) | $\approx 04 \text{ Hz}$ |
| 4 | Source-to-substrate distance | $\approx 38 \text{ mm}$ |
| 5 | Substrate temperature (T_s) | $300 \text{ K} \leq T_s \leq 675 \text{ K}$ |
| 6 | Thickness of thin films (d) | $\approx 100 \text{ nm}$ |
| 7 | Base vacuum | $\approx 1.00 \times 10^{-4} \text{ Pa}$ |
| 8 | Deposition time (laser ablation time) | 05-to-20 minutes |



spectrophotometer (model: Lambda 1050+, make: PerkinElmer, USA) in the 400 to 900 nm wavelength (λ) range. FTIR spectrophotometer (model: IRSpirit-X, make: Shimadzu, Japan) operated in mid-infrared mode at room temperature (RT) (≈ 303 K) in the wavenumber ($\bar{\nu}$) range 4000–400 cm^{-1} with a resolution of 2 cm^{-1} to spot the functional groups existing (if any) in the pulsed laser deposited CdIn_2Se_4 thin films deposited at various T_s .

The thin film characteristics altered depending on numerous pre- and post-deposition conditions. All other PLD parameters itemized in Table 1 were held constant during the current experiments, except for T_s and deposition duration, to ensure the reproducibility of the findings.

3 Results and discussion

3.1 UV-vis-NIR spectrophotometer analysis

The UV-VIS-NIR spectrophotometer was employed to derive optical spectra of T_s -modified CdIn_2Se_4 thin films. UV-VIS-NIR spectrophotometer can produce optical spectra in a variety of modes, including $T(\lambda)$, reflectance ($R(\lambda)$), and absorption ($A(\lambda)$), depending on the materials' structure and characteristics. An opaque sample, such as pellet, bulk, *etc.*, has awfully low transparency, often imminent to zero (≈ 0), and the optical parameters are resolute when measured by consuming the diffuse reflectance spectra (DRS), which use the $R(\lambda)$ spectra as per Kubelka–Munk (K–M) theory.³⁸ According to Jubu *et al.*,³⁹ the Tauc technique evaluates the optical characteristics of a transparent sample by using the absorption ($A(\lambda)$) and/or $T(\lambda)$ spectra of the UV-VIS-NIR spectrophotometer.

The current study analyzes λ -dependent room temperature (RT) (≈ 300 K) $T(\lambda)$ spectra, Fig. 1, for T_s tempered CdIn_2Se_4 thin films using a UV-VIS-NIR spectrophotometer in the λ range of 400 to 900 nm.

The shift in λ dependent $T(\lambda)$ maxima perceptible in Fig. 1 can be explained by the thin films of the CdIn_2Se_4 formed at low T_s ($T_s < 425$ K) have dispersed microcrystallites, random orientation, disordered grain boundaries, and are essentially

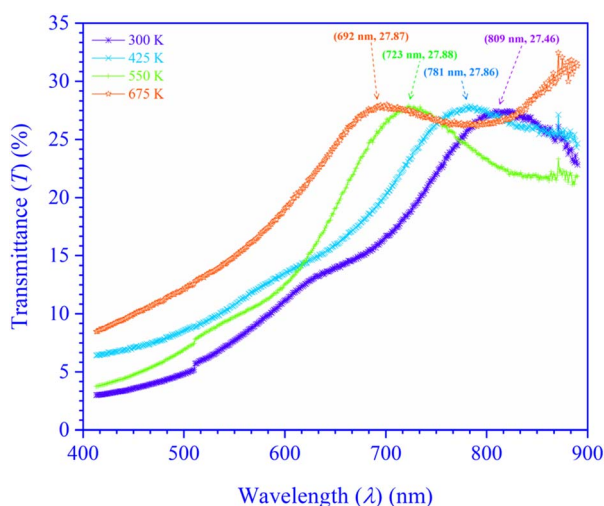


Fig. 1 Transmittance spectra of T_s -moderated CdIn_2Se_4 thin films.

amorphous, which contributes to lower $T(\lambda)$ and increased absorption ($A(\lambda)$). Conversely, CdIn_2Se_4 thin films grown at higher T_s ($300 \text{ K} < T_s < 675 \text{ K}$) have a stronger orientation, organized microcrystallites, starkly defined grain boundaries, and are essentially polycrystalline, all of which contribute to elevated $T(\lambda)$ and diminished absorbing ($A(\lambda)$) capabilities. When deposited at 675 K T_s (>550 K), thin films of the CdIn_2Se_4 show an additional phase (In_2Se_3)⁴⁰ that could be the cause of the $T(\lambda)$ and absorption ($A(\lambda)$) divergence. The characteristic wavelengths (λ_c) of T_s modified CdIn_2Se_4 thin films with their $T(\lambda)$ amplitude are revealed in Fig. 1. The T_s modulated CdIn_2Se_4 thin films has high absorption in the visible region with a hump at 750.00 ± 58.50 nm making it a good choice for light absorbing material.

Using eqn (1)–(3), Fig. 2 demonstrates how the optical parameters—the absorption coefficient (α), refractive index (η), and extinction coefficient (k)—vary with λ for T_s curbed CdIn_2Se_4 thin films.

$$\alpha = \frac{2.303 \times A}{d} \quad (1)$$

$$\eta = \frac{1 + \sqrt{R}}{1 - \sqrt{R}} \quad (2)$$

$$k = \frac{\alpha \lambda}{4\pi} \quad (3)$$

Eqn (1) shows that the d is ≈ 100 nm for CdIn_2Se_4 thin films.

The α scale depends upon radiation photon energy ($h\nu$) and the structure of a thin film. Bulk and/or thin films with higher α absorb photons more readily, which excite electrons into the conduction band (CB). The higher value of α ($\approx 10^7 \text{ m}^{-1}$)^{32,41} of T_s curbed CdIn_2Se_4 thin films palpable in Fig. 2(a) supports the direct optical band gap (E_g) nature of the semiconductor³² and makes it a very good candidate for designing and developing opto-electronic devices.⁴²

Fig. 2(b) shows $R(\lambda)$ dependent η ($= \frac{1 + R^{0.5}}{1 - R^{0.5}}$) spectra as a function of λ for T_s -controlled CdIn_2Se_4 thin films. The dispersion curves of the η show crests at λ_c , which the oscillator model can explain. As per El-Nahass *et al.*,⁴³ at a λ higher than the λ_c , the spectral behavior of the η parades normal dispersion, which the single oscillator model can explicate. The η values deduced for T_s tempered CdIn_2Se_4 thin films, stake well with the empirical relation $\eta^4(E_g - 0.365) = 154$ ($\eta \approx 3.27$) agreed by Reddy *et al.*^{31,44,45}

The k quantifies the percentage of light energy lost through scattering and/or absorption per unit transit distance in thin films, reflecting the absorption of electromagnetic waves due to inelastic scattering events. Through empirical observation, the k is proportional to the α ($= \frac{\alpha \lambda}{4\pi}$). Fig. 2(c) shows the change in k with λ for T_s modified CdIn_2Se_4 thin films. The k decreases with an increase in λ and reaches a minimum at λ_c ; the increment in k values after λ_c can be elucidated due to the free carrier



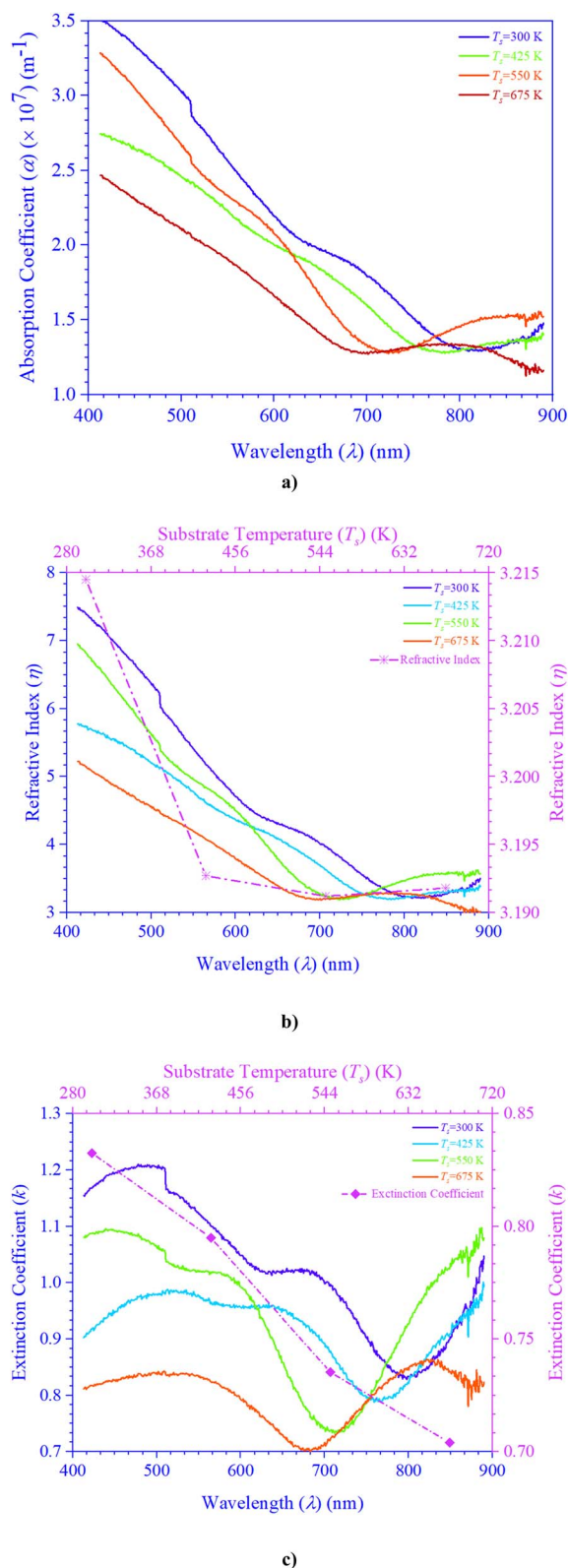


Fig. 2 T_s modulated CdIn_2Se_4 thin films' (a) absorption coefficient, (b) refractive index, and (c) extinction coefficient.

absorption contribution; the behavior agrees well with the results reported by El-Nahass *et al.*^{43,45}

The course used to synthesize the bulk and/or thin film, the thickness of the bulk and/or thin film (d), T_s at which thin films were/are grown, *etc.*, could all be causative factors to the variation in the α , η , and k values for the bulk and/or thin film CdIn_2Se_4 .

To reach the lowest energy optically excited state, the incident photon energy ($h\nu$) is designated by the optical band gap (E_g). The Tauc technique construes the E_g of T_s , moderated CdIn_2Se_4 thin films. The optical α is correlated to the E_g for interband transitions in a semiconductor, adjacent to the E_g by engaging eqn (4).⁴⁶

$$(\alpha h\nu)^{\frac{1}{n}} = A(h\nu - E_g) \quad (4)$$

In eqn (4), the transition probability is symbolized by n ($=2, 1/2, 2/3$, and $1/3$ for direct allowed, indirect allowed, direct forbidden, and indirect forbidden transitions, respectively), and A is a constant that is contingent on the nature of the transition.

Photons have less energy than the band gap; therefore, materials in any form—bulk or thin film—cannot absorb light beneath it. Fig. 3 shows the plot of $(\alpha h\nu)^2$ vis-à-vis photon energy ($h\nu$), which is used to find the E_g values of T_s curved CdIn_2Se_4 thin films. The direct E_g values may be articulated by extrapolating the straight segment of the graphs at the values where $(\alpha h\nu)^2$ tends to zero (≈ 0).

The E_g values of the thin films grown below 550 K T_s (<550 K) *i.e.* at 300 K and 425 K are found to be ≈ 1.53 eV and ≈ 1.59 eV, which are slightly less than the CdIn_2Se_4 's reported direct E_g value ≈ 1.67 eV attainable for pure α -phase CdIn_2Se_4 crystal derived by optical absorption method at 293 K temperature.¹⁹ Nevertheless, CdIn_2Se_4 thin films grown at 550 K T_s (≈ 550 K) have an E_g value (≈ 1.72 eV) which is more or less equal to the reported bulk value. At higher T_s (>550 K), the higher value of the E_g (≈ 1.79 eV) can be explained by the dissociation of CdIn_2Se_4 thin film.⁴⁰ The E_g value increases with the T_s increase.

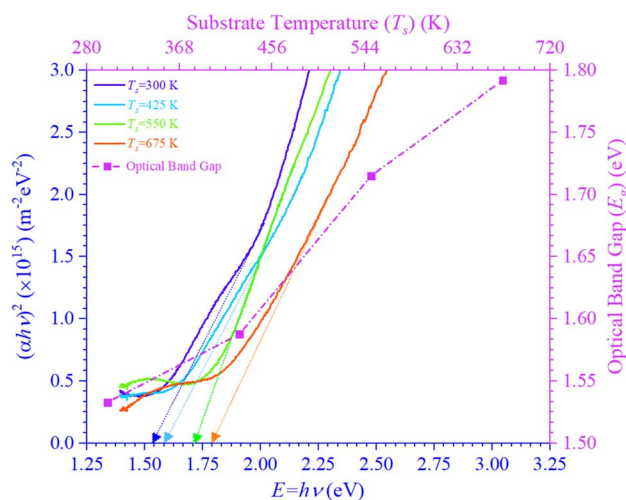


Fig. 3 Dependency of $(\alpha h\nu)^2$ on the photon energy for T_s -controlled CdIn_2Se_4 thin films.



As the T_s of CdIn₂Se₄ thin films rose, as ostensible in Fig. 1, $T(\lambda)$ changed toward higher energy ($=h\nu$), signifying that the optical band gap energy widened concurrently. The increase in E_g with increase in T_s may be explained due to the higher T_s providing atoms greater energy to rearrange into well-ordered crystal structures, they diminish grain boundaries and dislocations, which typically bring localized energy states within the E_g . Larger grain sizes in polycrystalline films frequently result from higher T_s ; dominating grain growth improves electronic properties and widens the E_g .^{47–51} The E_g value construed in the present investigation advocates that 550 K T_s deposited CdIn₂Se₄ thin films are hypothetically adequate for thin film solar cell applications.⁵²

There is diversity in the literature about the type of electronic transition and the corresponding E_g values. The E_g values of T_s tempered CdIn₂Se₄ thin films determined in the present investigation differ when compared with the literature survey,^{23,24,45,52,53} the incongruities explicated may be due to the individual or combined consequence of some factors like incongruent nature of the melting of CdIn₂Se₄, innumerable methods employed for synthesizing the compound and/or thin film deposition, T_s , an aberration in bulk and/or thin film's stoichiometry, charge impurities at the grain boundaries, lattice strain present in bulk and/or thin film, extent of structural disorder, etc.

The imaginary (IDC) (ϵ_i) and the real (RDC) (ϵ_r) dielectric constants are portions of the complex optical dielectric function; the IDC epitomizes the absorption of energy (E) from an electric field (F_e), which may be pronounced due to the motion of a dipole, while the RDC embodies the capacity of materials to lessen the speed of light (c); IDC and RDC have unswerving kin with the η and k . Fig. 4 displays the relationship between energy and the changes in the IDC ($=2\eta k$) (Fig. 4(a)), RDC ($=\eta^2 - k^2$) (Fig. 4(b)), and loss factor/dissipation factor/loss tangent ($\tan \delta$) ($= \frac{\epsilon_i}{\epsilon_r}$) (Fig. 4(c)) for T_s modified CdIn₂Se₄ thin films.

It is evident from Fig. 4 that IDC varies from 0.89×10^2 to 0.75×10^2 , RDC from -37.69 to 19.12 , and $\tan \delta$ from -2.37 to -3.92 with a change in T_s .

The negative values of the real dielectric constant (ϵ_r) indicate that the semiconductor materials reveal metallic behavior.⁵⁴

The rapport between E_g ($=h\nu$) and the vicissitudes in the natural logarithm of α ($\ln \alpha$), optical conductivity (σ_o), and electrical conductivity (σ_e) is revealed in Fig. 5. An alteration in optical state occurs when the valence band (VB) tail becomes occupied, and the conduction band (CB) edge becomes unoccupied, as revealed by eqn (5).⁵⁵

$$E_U \ln \frac{\alpha}{\alpha_0} = h\nu \quad (5)$$

In this context, α_0 represents an Urbach absorption coefficient (constant), and E_U , which stands for Urbach's energy, determines the slope of the exponential edge and can be seen as the width of the tail of localized states in the forbidden energy gap. The thermal vibrations of the lattice form the basis of the E_U .

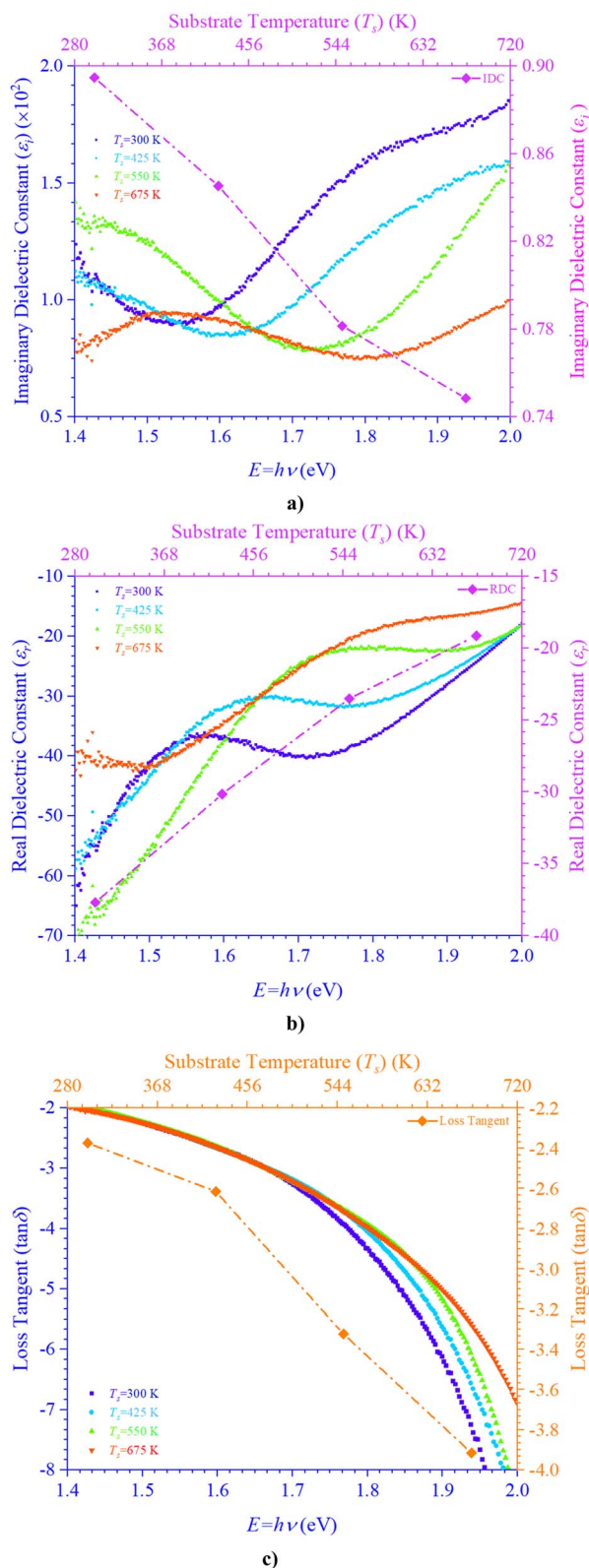


Fig. 4 Variation in (a) IDC, (b) RDC, and (c) $\tan \delta$ of CdIn₂Se₄ thin films as a function of energy.

The values of the E_U and α_0 attained from the $\ln \alpha$ against photon energy ($h\nu$) plot varies from 1.38 to 1.97 eV and 4.75×10^6 to 5.73×10^6 m⁻¹, respectively, with a change in T_s .



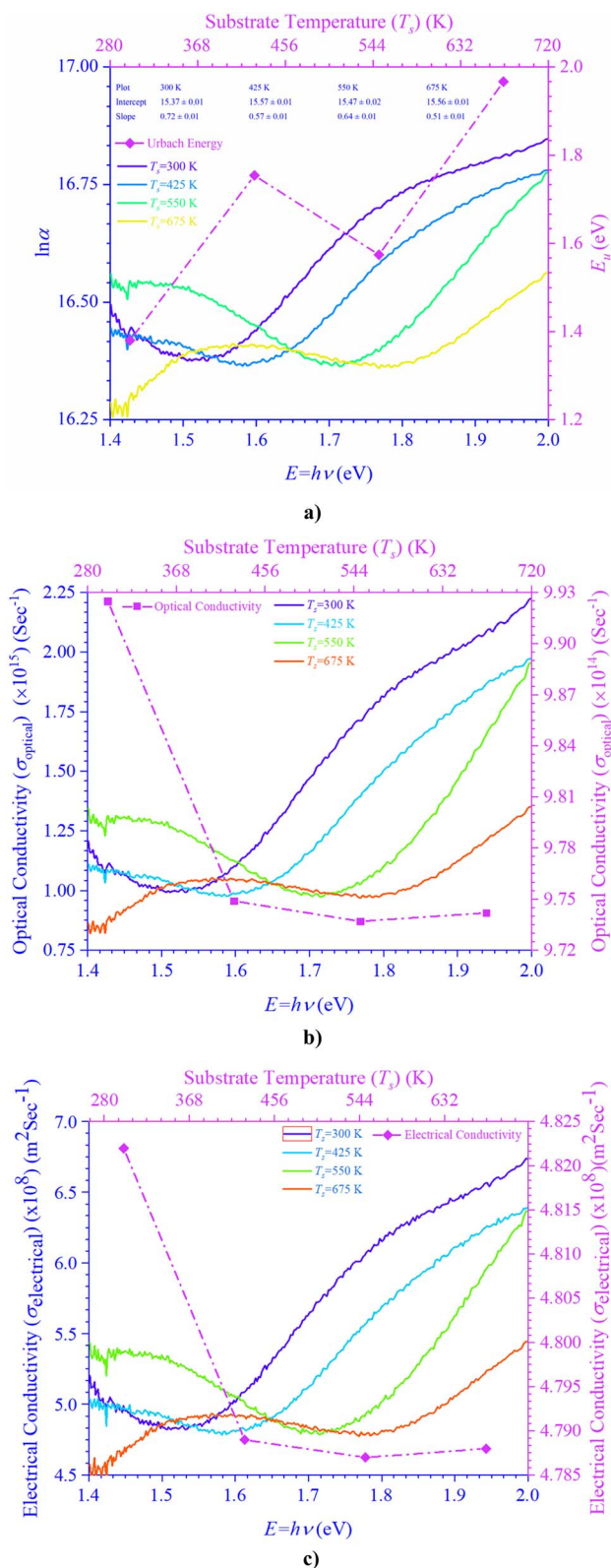


Fig. 5 Variation in (a) Urbach's energy, (b) optical conductivity, and (c) electrical conductivity of CdIn₂Se₄ thin films as a function of energy.

The high density of localized states inside the E_g , as implied by the enormous E_U value, reveals numerous structural flaws in sample.⁵⁵ The powerful probes, σ_o $\left(= \frac{\alpha\eta c}{4\pi} \right)$ and σ_e $\left(= \frac{2\pi\sigma_o}{\alpha} \right)$

represent the mobility of the charge carriers induced by the alternating electric field of the passing electromagnetic waves,⁵⁵ and are employed in investigating the electrical properties of different materials. The values of σ_o and σ_e for T_s curbed CdIn₂Se₄ thin films extracted at λ_c are plotted in Fig. 5(b) and (c), respectively.

The σ_e is reliant on σ_o , while σ_o is based on the α . As light absorption grows, σ_o and σ_e climb, enabling electrons to acquire more energy and become free for conduction.⁵⁶

Fig. 6 portrays IDC and RDC reliant volume (VELF) $\left(= \frac{\epsilon_i}{\epsilon_r^2 + \epsilon_i^2} \right)$ (Fig. 6(a)) and surface (SELF) $\left(= \frac{\epsilon_i}{(\epsilon_r + 1)^2 + \epsilon_i^2} \right)$ (Fig. 6(b)) energy loss functions depict electron and optical transitions in T_s , moderated

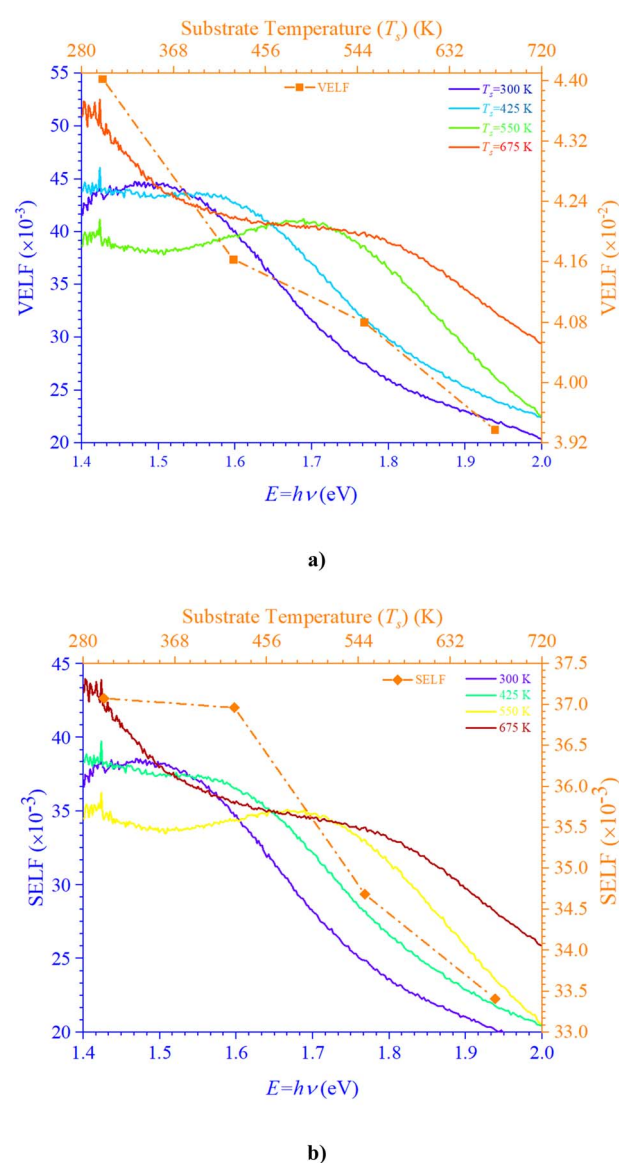


Fig. 6 Variation in (a) VELF and (b) SELF of CdIn₂Se₄ thin films as a function of energy.



CdIn₂Se₄ thin films. The VELF and SELF are used to weigh the energy loss rates of electrons as they move across most of the surface. The peak values of VELF and SELF for T_s curbed CdIn₂Se₄ thin films extracted at λ_c vary from 44.03×10^{-3} to 39.37×10^{-3} and 37.08×10^{-3} to 33.41×10^{-3} , respectively.

3.2. FTIR spectrophotometer analysis

The room temperature (RT) (≈ 300 K) FTIR spectra of T_s controlled CdIn₂Se₄ thin films recorded in the 4000 to 400 cm^{-1} wavenumber ($\bar{\nu}$) range is offered in Fig. 7.

In synthesizing CdIn₂Se₄, only 5N (99.999%) pure Cd, In, and Se were employed; no other chemicals or chemical routes were used, and a non-chemical approach was used to deposit CdIn₂Se₄ thin films.

A peak perceived in T_s tempered CdIn₂Se₄ thin films between 880–892 cm^{-1} wavenumber ($\bar{\nu}$) can be construed due to bending C=C and/or C–H functional groups and alkene and/or 1,2,4-trisubstituted and/or 1,3-disubstituted class. A peak seized between 757 and 760 cm^{-1} wavenumber ($\bar{\nu}$) can be interpreted due to stretching C–Cl and halo compound functional group, and/or bending C=H functional group and 1,2-disubstituted or monosubstituted class. The absorption peaks due to C=C, C–H, and/or C–Cl functional group/s habitually parade a stout absorption edge in the FTIR spectra if existing in the T_s modified CdIn₂Se₄ thin films. The absorption edges are evident in the T_s controlled CdIn₂Se₄ thin films' FTIR spectra between 880–892 cm^{-1} and 757–760 cm^{-1} wavenumbers ($\bar{\nu}$), but they are frail; henceforth, it may be concluded that the T_s moderated CdIn₂Se₄ thin films are intrinsic and free from any functional group.^{21,57} The shift in wavenumber ($\bar{\nu}$) dependent absorbance (A) maxima conspicuous in Fig. 7 can be explained by the amorphous, polycrystalline, and polyphase nature of the T_s controlled CdIn₂Se₄ thin films. Peaks in FTIR spectra of T_s tempered CdIn₂Se₄ thin films at wavenumbers ($\bar{\nu}$) 3437.74 ± 49.87 cm^{-1} , 1658.41 cm^{-1} , and 1597.77 ± 23.32 cm^{-1} are detected and dispensed by the instrument, but their amplitude is impending almost to zero (≈ 0), so they are not identified and indexed.

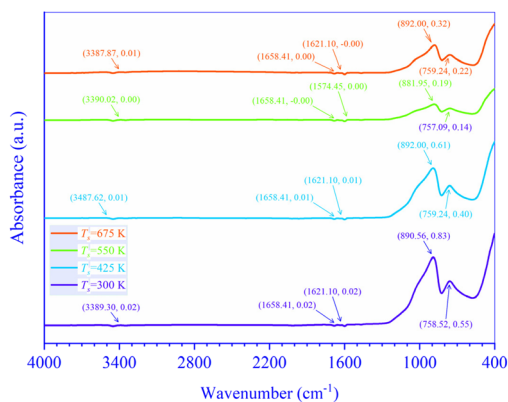


Fig. 7 FTIR spectra of T_s modified CdIn₂Se₄ thin films.

4 Conclusions

The optical characterization of the PLD technique deposited ≈ 100 nm thick CdIn₂Se₄ thin films on amorphous quartz glass at mixt T_s was carried out by recording RT $T(\lambda)$ spectra in the 400 to 900 nm λ range using a UV-Vis-NIR spectrophotometer. A shift in T_s modulated CdIn₂Se₄ thin film's $T(\lambda)$ maxima is evident and exhibits high absorption in the visible region with a hump at 750.00 ± 58.50 nm and depicts α of the order of $\approx 10^7$ m^{-1} . The η values deduced for T_s tempered CdIn₂Se₄ thin films (≈ 3.27). The k decreases with an increase in λ and reaches a minimum at λ_c . Because of their amorphous nature, the E_g of CdIn₂Se₄ thin films grown below 550 K T_s is slightly lower than the published value; while the polycrystalline thin films of CdIn₂Se₄ made at a T_s of 550 K have an E_g value that is approximately equal to the reported bulk value, the polyphase structure of the CdIn₂Se₄ thin film at higher T_s explains greater values of the E_g . For T_s -modulated CdIn₂Se₄ thin films, IDC, RDC, and $\tan \delta$, dependent on η and k have all been determined and compared with the reported data. The values of the E_U , α_0 , σ_0 , σ_e , VELF, and SELF of CdIn₂Se₄ thin films limited by T_s were retrieved at λ_c . The purity of CdIn₂Se₄ thin films formed at different T_s was verified by recording the FTIR spectra. The conclusions drawn from our extensive research include that the T_s -dependent optical parameters obtained in this study will aid in developing upcoming thin film electronic devices in which CdIn₂Se₄ thin film is one of the semiconducting materials. The impact of thin film d on the optical characteristics of CdIn₂Se₄ thin films deposited by PLD has not been investigated by researchers worldwide, despite the conclusion that this is a topic of future research. Research on compounds based on the II–III₂–VI₄ group in silicon-based microelectronic devices is underway. However, no attempt has been made to create a junction between silicon and CdIn₂Se₄, so the results of this study may provide insight into the development of new silicon-based microelectronic devices in the future. Additionally, the current research suggests that CdIn₂Se₄ thin films are potential choices for designing and developing future high-efficiency opto-electronic systems.

Data availability

The authors declare that the data supporting the findings of this study are available/included in the paper's main text.

Author contributions

All writers contributed to the study conception and design. Material preparation, data gathering, and analysis were accomplished by S. D. Dhruv, Tanvi Dudharejiya, Sergei A. Sharko, Aleksandra I. Serokurova, Nikolai N. Novitskii, D. L. Goroshko, Parth Rayani, Jagruti Jangale, Vanaraj Solanki, P. B. Patel, U. B. Trivedi, J. H. Markna, Bharat Kataria, and D. K. Dhruv. D. K. Dhruv wrote the first draft of the manuscript, and all authors commented on previous versions. All authors read and permitted the final manuscript. S. D. Dhruv: methodology. Tanvi Dudharejiya: conceptualization. Sergei A. Sharko:



investigation. Aleksandra I. Serokurova: formal analysis. Nikolai N. Novitskii: *visualization*. D. L. Goroshko: writing-review & editing. Parth Rayani: software. Jagruti Jangale: validation. Vanaraj Solanki: data curation. P. B. Patel: resources. U. B. Trivedi: resources. J. H. Markna: software. Bharat Kataria: project administration. D. K. Dhruv: writing-original draft, supervision.

Conflicts of interest

The submitted work is the authors' original research work and has not been communicated elsewhere for publication. On behalf of all co-authors, I declare no conflict of interest.

Acknowledgements

The work was supported by the Department of Science & Technology (DST), Government of India, New Delhi (File number: DST/INT/BLR/P-36/2023) and Belarusian Republican Foundation for Fundamental Research (File number: F23INDG-005) under the India-Belarus Programme of Co-operation in Science & Technology (Joint Research Project). The authors thank the Sophisticated Instrumentation Centre for Applied Research and Testing (SICART), Vallabh Vidyanagar-388120, Anand, Gujarat, India, for providing discounted UV-Vis-NIR and FTIR spectrophotometer facilities.

References

- 1 F. Yu, X. Meng, J. Cheng, J. Liu, Y. Yao and J. Li, *J. Alloys Compd.*, 2019, **797**, 940–944.
- 2 S. I. Radautsan, A. N. Georgobiani and I. M. Tiginyanu, *Prog. Cryst. Growth Charact.*, 1984, **10**, 403–412.
- 3 V. Dhamecha, B. Patel, D. Dhruv and A. Nowicki, *Surf. Eng.*, 2020, **36**, 100–105.
- 4 D. K. Dhruv, A. Nowicki, B. H. Patel and V. D. Dhamecha, *Surf. Eng.*, 2015, **31**, 556–562.
- 5 Y. Ai, Y. Li, T. Li, R. Hou, Q. Wang, A. Habib, G. Shao and P. Zhang, *iScience*, 2024, **27**, 110422.
- 6 J. He, B. Li, J. Yu, L. Qiao, S. Li, X. Zu and X. Xiang, *Opt. Mater.*, 2020, **108**, 110231.
- 7 C. Ling, X. Ye, J. Zhang, J. Zhang, S. Zhang, S. Meng, X. Fu and S. Chen, *Sci. Rep.*, 2017, **7**, 27.
- 8 J.-F. Lambert, P. V. Huong, J. Limtrakul and J.-C. Launay, *J. Mol. Struct.*, 1993, **294**, 159–162.
- 9 P. Manca, F. Raga and A. Spiga, *Nuov. Cim. B*, 1974, **19**, 15–28.
- 10 S. S. Fouad, G. B. Sakr, I. S. Yahia and D. M. A. Basset, *Mater. Res. Bull.*, 2011, **46**, 2141–2146.
- 11 S. Ozaki, K.-I. Muto, H. Nagata and S. Adachi, *J. Appl. Phys.*, 2005, **97**, 043507.
- 12 Y. Ayeb, T. Ouahrani, R. Khenata, A. H. Reshak, D. Rached, A. Bouhemadou and R. Arrar, *Comput. Mater. Sci.*, 2010, **50**, 651–655.
- 13 P. Kumar, A. Soni, K. C. Bhamu and J. Sahariya, *Mater. Res. Bull.*, 2017, **86**, 131–138.
- 14 D. K. Dhruv, B. H. Patel, N. Agrawal, R. Banerjee, S. D. Dhruv, P. B. Patel and V. Patel, *J. Mater. Sci.: Mater. Electron.*, 2022, **33**, 24003–24015.
- 15 J. Sahariya, P. Kumar, A. Soni and K. C. Bhamu, *Macromol. Symp.*, 2017, **376**, 1600203.
- 16 D. K. Dhruv, B. H. Patel and D. Lakshminarayana, *Mater. Res. Innovations*, 2016, **20**, 285–292.
- 17 F. J. García and M. S. Tomar, *Thin Solid Films*, 1980, **69**, 137–139.
- 18 H. Hahn, G. Frank, W. Klingler, A. D. Störger and G. Störger, *Z. Anorg. Allg. Chem.*, 1955, **279**, 241–270.
- 19 O. Madelung, *Semiconductors: Data Handbook*, Springer Berlin Heidelberg, Berlin, Heidelberg, 2004.
- 20 K. Adpakpang, T. Sarakonsri, S. Isoda, Y. Shinoda and C. Thanachayanont, *J. Alloys Compd.*, 2010, **500**, 259–263.
- 21 A.-A. Ruanthon, T. Sarakonsri and C. Thanachayanont, *Funct. Mater. Lett.*, 2009, **2**, 199–203.
- 22 V. M. Nikale, S. S. Shinde, A. R. Babar, C. H. Bhosale and K. Y. Rajpure, *Sol. Energy*, 2011, **85**, 325–333.
- 23 V. M. Nikale, S. S. Shinde, A. R. Babar, C. H. Bhosale and K. Y. Rajpure, *Sol. Energy*, 2011, **85**, 1336–1342.
- 24 V. M. Nikale, S. S. Shinde, A. R. Babar, C. H. Bhosale and K. Y. Rajpure, *Appl. Sol. Energy*, 2010, **46**, 194–201.
- 25 R. Tenne, Y. Mirovsky, G. Sawatzky and W. Gariat, *J. Electrochem. Soc.*, 1985, **132**, 1829–1835.
- 26 M. Tomkiewicz, W. Siripala and R. Tenne, *J. Electrochem. Soc.*, 1984, **131**, 736–740.
- 27 L. Fornarini, F. Stirpe, E. Cardarelli and B. Scrosati, *Sol. Cells*, 1984, **11**, 389–400.
- 28 R. Tenne, Y. Mirovsky, Y. Greenstein and D. Cahen, *J. Electrochem. Soc.*, 1982, **129**, 1506–1512.
- 29 V. Nikale, *Sol. Energy Mater. Sol. Cells*, 2004, **82**, 3–10.
- 30 A. Priyambada, A. Mohanty and P. Parida, *Mater. Today Commun.*, 2023, **37**, 107338.
- 31 D. M. Hoat, M. Naseri, R. Ponce-Pérez, J. F. Rivas-Silva and G. H. Coccoletzi, *J. Solid State Chem.*, 2020, **282**, 121078.
- 32 D. Sudha, S. Dhanapandian, C. Manoharan and A. Arunachalam, *Results Phys.*, 2016, **6**, 599–605.
- 33 D. Santamaría-Pérez, O. Gomis, A. L. J. Pereira, R. Vilaplana, C. Popescu, J. A. Sans, F. J. Manjón, P. Rodríguez-Hernández, A. Muñoz, V. V. Ursaki and I. M. Tiginyanu, *J. Phys. Chem. C*, 2014, **118**, 26987–26999.
- 34 V. M. Nikale, S. S. Shinde, C. H. Bhosale and K. Y. Rajpure, *J. Alloys Compd.*, 2011, **509**, 3116–3121.
- 35 P. D'Agosta, F. Tumino, V. Russo, A. Li Bassi and C. S. Casari, *Nanoscale*, 2023, **15**, 7493–7501.
- 36 H. Liang, J. Tan, Y. Chen, Y. Ma, X. Guan, Y. Zou, Y. Zhou, Z. Zheng, W. Huang, C. Du, G. Ouyang, J. Yao and G. Yang, *Nano Mater. Sci.*, 2025, S258996512500056X.
- 37 S. D. Dhruv, S. A. Sharko, A. I. Serokurova, N. N. Novitskii, D. L. Goroshko, P. Rayani, J. Jangale, N. Agrawal, V. Solanki, J. H. Markna, B. Kataria and D. K. Dhruv, *RSC Adv.*, 2025, **15**, 14859–14875.
- 38 M. Patel, A. Chavda, I. Mukhopadhyay, J. Kim and A. Ray, *Nanoscale*, 2016, **8**, 2293–2303.
- 39 P. R. Jubu, F. K. Yam, V. M. Igba and K. P. Beh, *J. Solid State Chem.*, 2020, **290**, 121576.



- 40 S. M. Patel and M. H. Ali, *Mater. Lett.*, 1987, **5**, 350–356.
- 41 J.-H. Ahn, G. Cai, R. S. Mane, V. V. Todkar, A. V. Shaikh, H. Chung, M.-Y. Yoon and S.-H. Han, *Appl. Surf. Sci.*, 2007, **253**, 8588–8591.
- 42 G. Galzerano and P. Laporta, in *Encyclopedia of Condensed Matter Physics*, Elsevier, 2005, pp. 430–443.
- 43 M. M. El-Nahass, A. A. Attia, G. F. Salem, H. A. M. Ali and M. I. Ismail, *Phys. B*, 2013, **425**, 23–30.
- 44 R. R. Reddy and Y. Nazeer Ahammed, *Infrared Phys. Technol.*, 1995, **36**, 825–830.
- 45 T. Mahalingam, S. Thanikaikarasan, R. Chandramohan, K. Chung, J. P. Chu, S. Velumani and J.-K. Rhee, *Mater. Sci. Eng. B*, 2010, **174**, 236–241.
- 46 P. Makuła, M. Pacia and W. Macyk, *J. Phys. Chem. Lett.*, 2018, **9**, 6814–6817.
- 47 N. Aravind and M. C. Santhosh Kumar, *J. Mater. Sci.: Mater. Electron.*, 2023, **34**, 1718.
- 48 S. D. Dhruv, S. A. Sharko, P. Solanki, M. Vala, I. T. Thakker, B. Kataria and D. K. Dhruv, *Solid State Phenom.*, 2023, **350**, 115–124.
- 49 D. K. Dhruv and B. H. Patel, *Int. J. Appl. Sci. Eng. Res.*, 2013, **3**, 121–128.
- 50 D. K. Dhruv and B. H. Patel, *Int. J. Innov. Res. Electr., Electron., Instrum. Control Eng.*, 2015, **3**, 9–11.
- 51 S. M. Patel and M. H. Ali, *Mater. Lett.*, 1987, **5**, 350–356.
- 52 A. B. Bhalerao, B. G. Wagh, R. N. Bulakhe, P. R. Deshmukh, J.-J. Shim and C. D. Lokhande, *J. J. Photochem. Photobiol., A*, 2017, **336**, 69–76.
- 53 M. M. El-Nahass, *Appl. Phys. A*, 1991, **52**, 353–357.
- 54 I. Jamaï, M. Ziati, N. Bekkioui and H. Ez-Zahraouy, *Phys. Scr.*, 2024, **99**, 105936.
- 55 A. M. A. Henaish, H. M. H. Zakaly, H. A. Saudi, S. A. M. Issa, H. O. Tekin, M. M. Hessein and Y. S. Rammah, *J. Electron. Mater.*, 2022, **51**, 2070–2076.
- 56 M. M. Al-anazy, T. Zelai, A. Rahim, A. A. AlObaid, T. I. Al-Muhimeed, A. I. Aljameel, A. Mera, A. Dahshan, Q. Mahmood, G. Murtaza and G. Nazir, *J. Solid State Chem.*, 2021, **303**, 122480.
- 57 Z. H. Mahmoud, Y. Ajaj, A. M. Hussein, H. N. K. Al-Salman, M. A. Mustafa, E. H. Kadhum, S. Abdullaev, S. A. Khuder, G. K. Ghadir, S. M. Hameed, K. Muzammil, S. Islam and E. Kianfar, *Int. J. Biol. Macromol.*, 2024, **267**, 131465.

